UHASSELT
KNOWLEDGE IN ACTION

Maastricht University

Faculty of Medicine and Life Sciences
School for Life Sciences
Master of Biomedical Sciences

Master's thesis

Investigating reactive oxygen species in oral squamous cell carcinoma as a therapeutic target for an innovative nanocarrier drug delivery system

Quinn Croughs

Thesis presented in fulfillment of the requirements for the degree of Master of Biomedical Sciences, specialization Molecular Mechanisms in Health and Disease

SUPERVISOR :

Prof. dr. Esther WOLFS

MENTOR :

Mevrouw Nuran CAZ

2023
2024

Transnational University Limburg is a unique collaboration of two universities in two countries: the University of Hasselt and Maastricht University.

UHASSELT
KNOWLEDGE IN ACTION

www.uhasselt.be
Universiteit Hasselt
Campus Hasselt:
Martelarenlaan 42 | 3500 Hasselt
Campus Diepenbeek:
Agoralaan Gebouw D | 3590 Diepenbeek

UHASSELT
KNOWLEDGE IN ACTION

Maastricht University

Faculty of Medicine and Life Sciences
School for Life Sciences
Master of Biomedical Sciences

Master's thesis

Investigating reactive oxygen species in oral squamous cell carcinoma as a therapeutic target for an innovative nanocarrier drug delivery system

Quinn Croughs

Thesis presented in fulfillment of the requirements for the degree of Master of Biomedical Sciences, specialization Molecular Mechanisms in Health and Disease

SUPERVISOR :

Prof. dr. Esther WOLFS

MENTOR :

Mevrouw Nuran CAZ

Investigating Reactive Oxygen Species in Oral Squamous Cell Carcinoma as a Therapeutic Target for an Innovative Nanocarrier Drug Delivery System*

Quinn Croughs[1], Nuran Caz[1], Sourav Nayak[2], Anitha Ethirajan[2] and Esther Wolfs[1]

[1]Laboratory for Functional Imaging & Research on Stem Cells (FIERCE), Biomedical Research Institute, Universiteit Hasselt, Campus Diepenbeek, Agoralaan Gebouw C - B-3590 Diepenbeek

[2]Nanobiophysics and Soft Matter Interfaces (NSI), Institute for Materials research (IMO-IMOMEC), IMEC, Universiteit Hasselt, Wetenschapspark 1 3590 Diepenbeek

*Running title: *Targeting oral cancer using smart nanocarriers*

To whom correspondence should be addressed: Prof. dr. Esther Wolfs, Tel: +32 (11) 26 92 96; Email: esther.wolfs@uhasselt.be

Keywords: oral squamous cell carcinoma, redox balance, nanocarrier, targeted drug delivery, cisplatin

ABSTRACT

Oral squamous cell carcinoma (OSCC) ranks as the 6th most prevalent cancer worldwide. The standard cisplatin chemotherapy is associated with systemic toxicity, limiting the therapeutic potential. Nanocarriers (NCs), a novel class of nanomedicines, aim to overcome off-target effects by encapsulating a drug of choice and releasing this cargo upon specific stimuli. The cellular redox status can be exploited as a stimulus through the incorporation of reactive materials in the NC shell, thereby increasing the specificity. We investigated the redox status in a cell line of OSCC and its potential as a stimulus to release cisplatin from our NCs. While confocal imaging indicated successful uptake and cargo release of the NCs, viability assessment of OSCC exposed to cisplatin-loaded NCs showed that the drug-loading capacity (DLC) was insufficient to induce apoptosis. Therefore, current efforts will focus on increasing the DLC in the ongoing process of NC optimization. We used a variety of reactive-oxygen-species (ROS) and glutathione (GSH) reporting fluorescent probes to visualize the redox status *in vitro,* and have indicated elevated levels of ROS in OSCC. Further optimization is required to gain more insights in the redox status and to apply these insights to the NC optimization. Once optimized, the NCs may be tested *in vivo* and are expected to decrease off-target effects while maintaining high efficiency in eliminating OSCC. If successful, this therapy would contribute to the quality-of-life of OSCC patients.

INTRODUCTION

Head and neck cancers are a group of malignancies that pose a major global concern, with 900.000 to 1.000.000 new cases being diagnosed annually (1). Malignancies in the head and neck area arise predominantly (approx. 90%) from the mucosal surfaces in the oral or nasal cavity, in the paranasal sinuses, or in the pharyngeal region and are referred to as head and neck squamous cell carcinomas (HNSCC) (2, 3). Patients may experience discomfort due to painful lumps and swellings, causing difficulty with speaking, eating, or breathing depending on the anatomical site, and size of the primary tumor (4). The most prominent risk factors for developing HNSCC include the use of tobacco (either smoking or chewing) and the consumption of alcohol, together accounting for up to 75% of HNSCC cases across Western Europe and the United States (3, 5). Infection with the human papillomavirus (HPV) is a third major risk factor that results in HPV-positive HNSCC (3, 5). This latter type of HNSCC is associated with an improved response to radio- and immunotherapy and, therefore, a better prognosis compared to HPV-negative HNSCC (2, 3, 5). The more complex HPV-negative type of HNSCC shows significantly increased inter- and intratumoral heterogeneity and a higher diversity in treatment response, highlighting the importance of research efforts towards better treatment options (6).

A variety of therapeutic options are currently available depending on the type, location, and stage of the cancer. Over 60% of patients are diagnosed with late-stage (III-IV) HNSCC, for whom surgical resection by itself no longer provides a good long-term survival prognosis due to surgical complications, local recurrence, and distant metastases (2). For these patients, a multimodal approach consisting of surgical resection considering the feasibility, followed by definitive chemoradiotherapy with cisplatin as the preferred chemotherapeutic agent for HNSCC, is considered the standard-of-care with established survival benefits (2, 7). Despite these survival benefits, the use of cisplatin is associated with both short- and long-term systemic toxicities, thereby limiting the therapeutic potential and decreasing the quality of life for the patient (2, 8, 9). The main dose-limiting factor for the treatment involves the nephro- and neurotoxic effects of cisplatin that occur in the majority of patients. Patients may develop renal failure due to accumulation of cisplatin in the kidney, along with paresthesia and painful/burning sensations caused by damage on peripheral nerves and dorsal root ganglia. Other adverse effects from cisplatin therapy include gastrointestinal toxicity, myelosuppression, and ototoxicity (8-11). These toxic effects are dose-dependent and may become irreversible over time. Taken together, these complications of freely-administered cisplatin severely impact the health and general quality of life of the patients. This highlights the importance of alternative therapeutic strategies that spare the patient from systemic toxicity, while maintaining high efficacy in tumor elimination.

The application of nano-structures in medicine holds great promise towards these alternative therapies and advanced healthcare applications. The enhanced pharmacodynamic and -kinetic profiles that nanomedicines offer, aim to minimize local and systemic side effects, and increase therapeutic efficacy (12). Extensive research is performed to design and develop these therapies for diseases where the current standard of care is lacking, as is the case for cancer therapy (13-15). Nanocarriers (NCs) are an emerging category of selective drug carrier and delivery systems among nanomedicines, which may offer an opportunity to treat cancers, including HNSCC, in a targeted and controlled approach (13, 15). A range of NC drug delivery systems are in the pipeline for cancer research, varying in structural basis and targeting mechanism (13-15). The principle is based on a nano-sized structure (liposomes, (bio)polymeric nanoparticles, dendrimers, etc.) that encapsulates and protects a drug from degradation until it reaches its target site, where it responds to a stimulus in order to release the content (13, 15). These NCs have the advantage of increased solubility and bioavailability, improved stability, and decreased toxicity (12). The NCs can reach their target site through a variety of active or passive mechanisms. Firstly, the leaky vasculature and poor lymphatic system of the tumor allows the NCs to passively accumulate in the tumor tissue, through the enhanced permeability and retention (EPR) effect (16). However, due to the variability of this effect caused by tumor heterogeneity, therapies solely based on EPR show widespread

clinical responses (17). Therefore, newer generation NCs aim to increase tissue- and cell-specific accumulation through active targeting approaches by incorporating a variety of receptor ligands in the NC shell. To date, these approaches are limited in clinical translation due to insufficient knowledge of the ligand-coupled NCs, along with concerns for off-target receptor binding (12-15). Besides ligand conjugation, the NC shell can be modified to optimize the drug-release stimulus. Controlled drug release by exogenous stimuli can be achieved through e.g. exposure to ultrasound, temperature or magnetic fields (13). These exogenous stimuli have to reach the NCs in order to induce drug-release, which may prove challenging, depending on the anatomical location and penetration depth of the stimulus (18). The drug-release stimulus can also be endogenous to the cancer tissue such as pH, redox status, enzyme activity, or temperature. Multiple promising pH-responsive NCs are already in the experimental phase for cancer treatment (19). These signals are inherent to the tumor microenvironment (TME) and allow to increase tissue-specificity, thereby enabling a safe and controlled delivery of drugs to the tumor.

The redox status of the TME emerges as another interesting target for the controlled release of NC cargo, since this equilibrium is dysregulated in cancer tissue. Through repeated carcinogen exposure, the normal mucosal surface progresses to phases of tissue hyperplasia, dysplasia and eventual carcinoma, accompanied by an increase in genetic instability over time (4). The progression through the different phases is marked by either loss or mutation of tumor suppressor gene regions, critical among them, the site of TP53 (4). In particular, loss of functional p53 in HNSCC is associated with increased production of reactive oxygen species (ROS) both in the malignant and non-malignant cells that reside in the TME (20, 21). These elevations of ROS in the tumor tissue are markedly different from normal ROS production in healthy tissue, and play an important part as signaling molecules where they contribute to drive carcinogenesis through cellular stress signaling. The elevated ROS can activate pathways involved in proliferation, genomic instability, inflammation, apoptosis resistance, and metabolic reprogramming, which all contribute to tumor growth and survival (20, 21). Elevations of ROS are also shown to stimulate angiogenic and metastatic pathways (22, 23). However, excessive levels of ROS can be toxic to the cancer cells, as they damage lipids, protein, and DNA. Therefore, the malignant cells also express elevated levels of antioxidant proteins, which protect the cellular structures and prevent ROS-induced apoptosis (24). The most prominent regulator of the intracellular redox balance is the glutathione (GSH) antioxidant system, which is also shown to be elevated in tumor tissue (25). Together, these antioxidant systems help to maintain redox balance which allows the cancer cells to exhibit tumor promoting signaling while sparing vital cellular structures from irreversible ROS-mediated damage. Despite its importance and potential as therapeutic target, current research efforts into detecting and quantifying the redox equilibrium in HNSCC are limited.

In this study, we aim to utilize the increased levels of ROS in the TME of HNSCC as a stimulus for the controlled release of cisplatin cargo from NCs, thereby minimizing the side-effects compared to free-administered cisplatin. To achieve this, we are developing and optimizing ROS-responsive NCs consisting of dextran biopolymers incorporated with thioketal linkers, which are chemical structures that are selectively cleaved in the presence of ROS (26, 27). The cleavage of these linkers leads to the degradation of the shell and release of the payload (28-30). This study also investigates and maps the presence of ROS and GSH in the TME to further understand the redox balance in malignant cells. A range of fluorescent ROS- and GSH-sensing probes were utilized *in vitro* to visualize the redox status. Taken together, the results of this study contribute to the development of an alternative and targeted therapy for HNSCC, potentially offering an increased quality of life by sparing the patients from the severe side-effects associated with the current standard-of-care.

EXPERIMENTAL PROCEDURES

Nanocarrier design and characterization – The NCs used in this study are composed of a dextran polysaccharide shell containing hydrophobic ROS-sensitive thioketal (TK-2COOH) linkers, synthesized by our colleague Sourav Nayak under supervision of Prof. Anitha Ethirajan (IMO, UHasselt). Briefly, TK-2COOH was first synthesized by mixing thioglycolic acid and acetone in an oven-dried flask with a catalytic amount of trifluoroacetic acid (TFA) (yielding 89% white product). Following, esterification of TK-2COOH with dextran in anhydrous dimethyl sulphoxide (DMSO) was conducted to prepare dextran-thioketal conjugates (DTKCs). After purification and dialysis steps, the conjugate was lyophilized and characterized. Gravimetric analysis and acid-base back titration were used to perform solubility tests and to determine free carboxylic acid groups for dextran-TK NCs. NCs were synthesized using the conjugate through inverse miniemulsion technique, as described in (31). Different hydrophilic payloads were loaded into the NCs and dynamic light scattering (DLS) was used to obtain the hydrodynamic diameter (D_h), which measured 145 nm for rhodamine-B loaded nanocarriers (RhoB-NCs) and 148 nm for cisplatin-loaded nanocarriers (Cis-NCs). The solid contents measured 7960 µg/ml and 7130 µg/mL and the polydispersity index (PDI) is 0.23 and 0.2 for the RhoB-NCs and the Cis-NCs respectively. The encapsulation efficiency was determined to be 86% for RhoB-NCs and >74% for Cis-NCs. Lastly, the drug loading content of our Cis-NCs measured 22.854 µg/mL NC dispersion in water.

Cell culturing – The human oral squamous cell carcinoma (OSCC) cell line UM-SCC-14C (CLS cell lines service, Germany, CVCL 7721) and the human keratinocyte (HaCaT) cell line (CLS cell lines service, Germany, CVCL 0038) were respectively cultured in Dulbecco's Modified Eagle Medium: nutrient mixture F-12 (DMEM/F-12 ,Gibco™, Thermo Fisher Scientific, Belgium) supplemented with 5% heat-inactivated fetal bovine serum (FBS, BioWest, Avantor, United States) and 1% penicillin/streptomycin (p/s), and DMEM (Gibco™, Thermo Fisher Scientific, Belgium) supplemented with 10% FBS and 1% p/s. Both cell lines were preserved in a humidified incubator at 37°C and 5% CO_2. Adherent OSCC and HaCaT were trypsinized using Accutase® solution (Sigma-Aldrich, Merck, Belgium) and TrypLE™ Express Enzyme (Gibco™, Thermo Fisher Scientific, Belgium) respectively. Prior to seeding, cells were counted using the trypan blue dye 0.4% (Gibco™, Thermo Fisher Scientific, Belgium) exclusion test.

Lentiviral vector construction, OSCC transduction – OSCC were transduced with a second-generation lentiviral vector system to incorporate the firefly luciferase (*Fluc*) gene. Lentiviral particles were produced in HEK293T cells as described in (32). Briefly, OSCC were seeded at $2{,}5x10^3$ cells/cm^2 and left to attach overnight. The cells were then exposed to the lentiviral particles for 7 days, followed by cell-selection through puromycin resistance (Invivogen, 1µg/mL administered every 3 days). This resulted in a transduced cell line of OSCC expressing the lentiviral vector with Fluc.

Cell viability assay – Cells were seeded at a density of $15x10^3$ cells/cm^3 and allowed for overnight adhesion. Following, the cells were treated either with rhodamine-b or cisplatin-containing NCs at different concentrations (10, 50, 100, 200, 500 µg/mL), or with free-dissolved cisplatin (Merck, Belgium) in a ratio of 1:1 or 7:3 DMSO:H_2O for 24h, 48h, and 72h. For ROS-experiments, both OSCC and HaCaT were seeded at the aforementioned cell density and treated with various concentrations of either tert-butylhydroperoxide (tBHP, VWR Chemicals, Belgium) or hydrogen peroxide (H_2O_2, VWR Chemicals, Belgium). Following the treatment periods, Alamar Blue (Bio-Rad, Belgium) protocol was performed according to the manufacturer's instructions. Fluorescence intensity was determined by using the CLARIOstar Plus microplate reader at 540/590 nm wavelength, (BMG Labtech, Germany). Data were normalized to the negative control and expressed as relative percentages.

Cellular uptake: fluorescent staining – Cells were seeded on glass coverslips at a density of $15x10^3$ cells/cm^3 and allowed for overnight adherence. Afterwards, OSCC were exposed to RhoB-NCs for 24h and 48h at 100 µg/mL and 200 µg/mL. Following incubation, cells were fixed using 4% paraformaldehyde (20 minutes, room temperature), followed by

staining with wheat germ agglutinin AlexaFluor 647 (WGA647, 1/200, Invitrogen™, Thermo Fisher Scientific, Belgium) for 10 min. Nuclear staining was performed by 10 min incubation with 4',6-diamidino-2-phenylindole (DAPI, 1/10000, Thermo Fisher Scientific, Belgium) in phosphate-buffered saline (PBS). The cells were mounted using Fluoromount mounting medium (Invitrogen™, Thermo Fisher Scientific, Belgium) on microscopic slides and left to dry overnight prior to imaging. High-resolution images were acquired using the LSM900 confocal microscope (Zeiss, Germany, LD C-Apochromat 40x/1.1 W Korr UV VIS IR). All images were processed using the ZEN Blue software.

Cellular uptake: *flow cytometry* – OSCC were seeded at a density of $23x10^3$ cells/cm^3 and were exposed to RhoB-NCs for 4h, 24h, and 48h at 100 µg/mL and 200 µg/mL. After the determined time of exposure, the cells were trypsinized, collected, and centrifuged at 2000 rpm for 5 minutes (room temperature). Cells were then washed with FACSbuffer (2% FBS in PBS) followed by fixation with 1 % paraformaldehyde (20 minutes, room temperature). A total of $10x10^3$ events were recorded using the LSRFortessa cell analyser (BD Biosciences). The Flowjo software was used to analyse and process the data.

Evaluation of redox status: microplate assays and live-cell microscopy – OSCC and HaCaT were seeded at a density of $15x10^3$ cells/cm^3. Following overnight adhesion, the cells were treated for 3h and 1h with various concentrations of either tert-butylhydroperoxide (tBHP, VWR Chemicals, Belgium) to induce oxidative stress, the ROS scavenger N-acetyl-L-cysteine (NAC, VWR Chemicals, Belgium), or a combination treatment. Next, the cells were incubated with ROS/GSH probes according to manufacturer instructions: The cell permeant reagent 2',7' – dichlorofluorescin diacetate (DCFDA, Abcam, Belgium, Ex/Em 485/535 nm) was used to detect cellular ROS activity. MitoSOX Red (Invitrogen™, Thermo Fisher Scientific, Belgium, Ex/Em 510/580 nm), and Peroxy-Orange1 (Merck, Ex/Em 543/600 nm) were used to specifically detect mitochondrial superoxide and cellular hydrogen peroxide respectively. Thioltracker Violet (Invitrogen™, Thermo Fisher Scientific, Belgium, Ex/Em 405/525 nm) was used to detect intracellular thiols. Lastly, the off-on fluorescent probe (NBD-P, synthesized as described in (33), Ex/Em 470/585 nm) was used to detect intracellular reduced GSH levels. The probe was diluted in PBS (final concentration 25 µM) and incubated for 30 minutes. Fluorescent signals were detected by CLARIOstar Plus microplate reader (BMG Labtech). Fluorescence intensity was normalized for cell density by sulforhodamine-B assay (SRB), as described in (34). Briefly, the cells were incubated with TCA-SRB (0.004% w/v SRB in 10% w/v TCA, 15 minutes, 4°C). Following incubation, the cells were washed with 1% acetic acid and incubated with Trizma base (10 mM, 5 minutes, room temperature). Fluorescence intensity was measured at 565/586 nm. Alternatively, fluorescent signals were imaged using the Zeiss LSM 880 at 37°C and 5% CO_2. All images were processed and analysed with FIJI (ImageJ).

Evaluation of redox status: flow cytometry – OSCC were grown in T75 culture flasks until 80% confluence. The cells were trypsinized as previously described and distributed in eppendorf tubes at 100.000 cells/tube. Following incubation with the aforementioned probe according to manufacturer instructions, the cells were treated as described above. Cells were left to incubate with ZombieNIR (Biolegend) for 20 minutes at 4°C to discern between live and dead cells. DCFDA signal intensity and frequency of parent was measured using the LSRFortessa (BD Biosciences, Belgium) in the FITC channel. FACS data was analysed using the FlowJo software.

Statistics – OSCC Graphpad Prism 10 was used for statistical analysis. Data is represented as mean ± SEM unless otherwise stated. Normality was checked using Shapiro-Wilk test. Normal data was analysed using one-way or two-way ANOVA, followed by Dunnett's or Tukey's multiple comparisons *post-hoc* as deemed appropriate. Statistical significance is indicated as *$p < 0,05$, **$p < 0,005$, ***$p < 0,001$, ****$p < 0,0001$.

RESULTS

ROS-responsive NCs do not induce cytotoxicity after successful uptake by OSCC – This first section describes the *in vitro* characterization of our designed NCs. To evaluate the biocompatibility and efficacy of ROS-responsive NCs to induce cell death in OSCC (n=3), an Alamar Blue cell viability assay was performed **(figure 1A-C).** NCs containing either rhodamine-B (NC-RhoB) or cisplatin in centrifugal or normal dispersion (NC-Cis CD and NC-Cis ND respectively) were administered in a range between 10-500 µg/mL for 24h and 48h, and compared to the untreated control. OSCC treated with NC-RhoB for 24h showed an increase in viability signal compared to the untreated control for every treatment condition, while the viability signal decreased in the 500 µg/ml condition after 48h of exposure (****p<0,0001) (**figure 1A)**. Similar effects were seen both for OSCC treated with NC-Cis CD or NC-Cis ND, following the 24h and 48h treatment **(figure 1B,C)**. These results indicate that the cisplatin cargo in the NCs is insufficiently concentrated to induce cell death in OSCC, and that the NCs structure in itself is biocompatible below exposure to 500 µg/mL. To assess cellular uptake of NCs, OSCC (n=3) were exposed to NC-RhoB for 24h and 48h and analyzed through flow cytometry **(figure 1D,E)**. Exposure to 200 µg/mL of NC-RhoB resulted in a higher percentage of positively stained OSCC compared to 100 µg/mL, in both the 24h and 48h conditions (****p<0,001 and ***p<0,00001 respectively) **(figure 1D)**. The representative histogram **(figure 1E)** indicates a shift in fluorescent RhoB signal associated with longer treatment duration and higher concentration. To verify that this increase is attributed to cellular uptake of NCs and not through interactions at the membrane level, confocal imaging was performed following exposure of OSCC (n=3) to NC-RhoB as previously described. Representative orthogonal images **(figure 1G)** indicate intracellular perinuclear presence of rhodamine-B after exposure to NC-RhoB 200 µg/mL for 24h and 48h (top and bottom respectively). Signal quantification indicated that the intracellular presence is increased at higher concentrations and longer incubation times of NCs **(figure 1F)** (****p<0,0001).

Cisplatin stability is unaffected by DMSO:H_2O solvent ratios but decreases over time of storage – We hypothesized that a mixture of DMSO and H_2O as a solvent could increase the drug-loading capacity of cisplatin without altering the NC structure. Therefore, we tested the stability of free-dissolved cisplatin in these conditions through an Alamar Blue viability assay of OSCC (n=3) exposed to a concentration range of 1µg/mL- 50µg/mL **(figure 2)**. Both a 1:1 and 7:3 DMSO:H_2O ratio of cisplatin solvent were tested as these were deemed viable ratios for the synthesis process. Our results show a decrease in cell viability compared to the untreated control following 24h of treatment with dissolved cisplatin (5 µg/mL: *p<0,05; 10-50 µg/ml: ****p<0,0001) for both 1:1 and 7:3 ratios **(figure 2A)** and **(figure 2D)** respectively. Similar effects are seen in the 48h and 72h condition, with a trend of decreasing viability associated with increased treatment duration **(figure 2B-C;E-F)**. To evaluate the stability of dissolved cisplatin, the samples were stored for one week in stable conditions and the experiment was repeated. Notably, when the OSCC are treated with the aged samples, the decreasing viability trend associated with increased treatment duration no longer appears **(figure 2B-C, E-F)**. At 24h after exposure to aged samples, the treated OSCC still indicate a decrease in viability compared to the untreated control (1:1 ratio 10 µg/mL: **p<0,005; 20-50 µg/mL: ****p<0,0001 // 7:3 ratio: 1-5 µg/mL: **p<0,005; 10-50µg/ml ****p<0,0001) (**figure 2A,D)**. However, following 72h, no treatment differences are observed for the aged samples, with the exception of 50 µg/mL in the 7:3 DMSO:H_2O ratio (****p<0,0001) (**figure 2F)**. To verify that all effects on cell viability can be attributed to dissolved cisplatin, we compared it to the vehicle control consisting of the 1:1 and 7:3 DMSO:H_2O solvent ratio's for fresh **(figure S1)** and aged **(figure S2)** samples, indicating no effect of solvent. These results indicate that the stability of cisplatin is unaffected by the ratio of DMSO:H_2O solvent, but decreases following sample storage. Taken together, these parameters will have to be taken in consideration in our ongoing NC optimization.

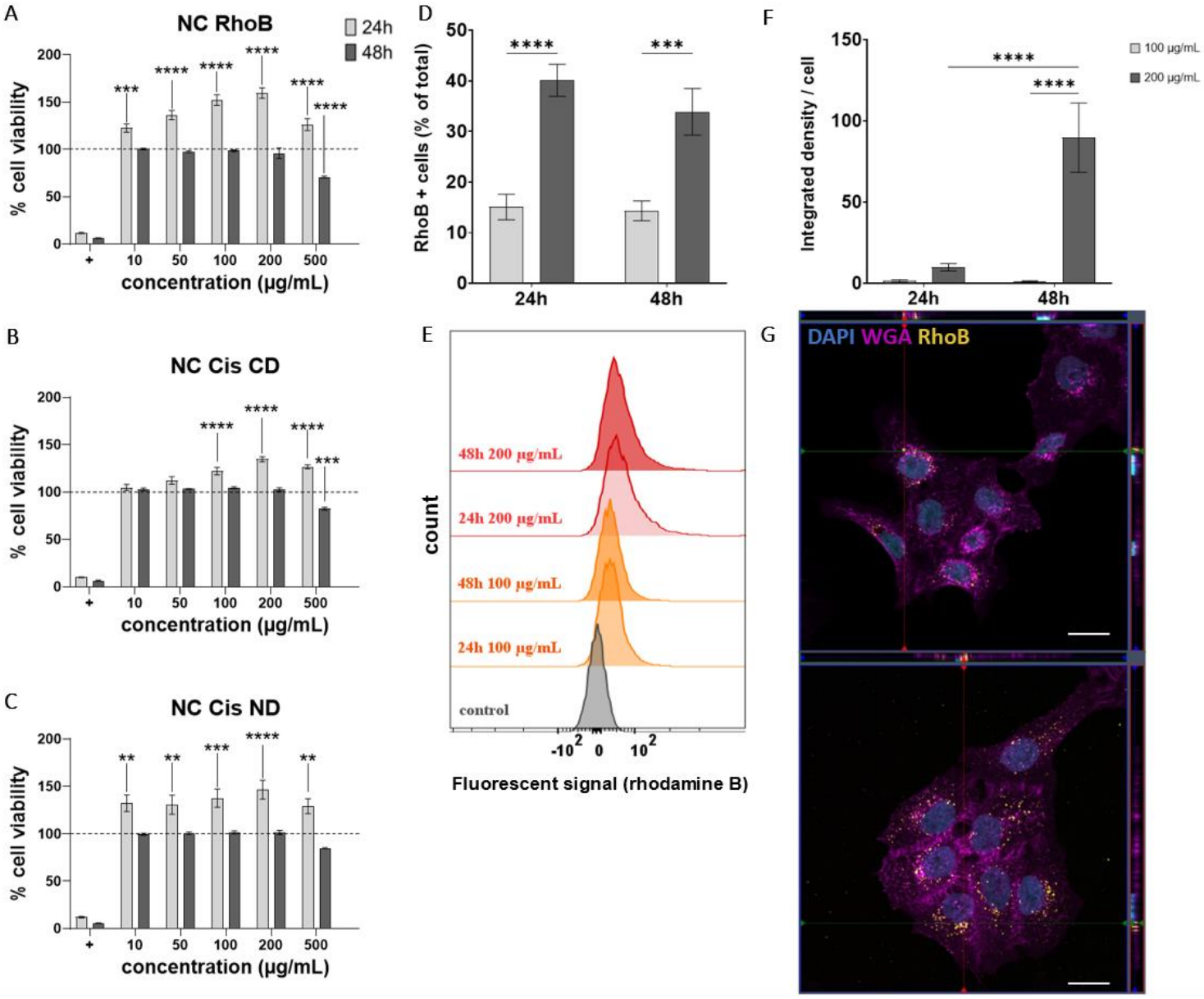

Fig.1 – ROS-responsive NCs do not induce cytotoxicity after successful cellular uptake. OSCC (n=3) were examined for cell viability using the Alamar Blue assay after incubation with different concentrations of ROS-responsive NCs, loaded with **(A)** Rhodamine-B, **(B)** Cisplatin through centrifugal dispersion, and **(C)** normal dispersion for a period of 24h and 48h. Data were normalized to the untreated control (dotted line) and expressed as relative percentages. NC-RhoB were assessed for uptake (% of total events per condition) through flowcytometry **(D)** following exposure of OSCC (n=3) to NC-RhoB at 100 µg/mL and 200 µg/mL for 24h and 48h. Representative histograms **(E)** indicating the mean fluorescent signal for the different NC-RhoB treatment conditions. Quantitative analysis of OSCC (n=3) exposed to NC-RhoB **(F)** at 100 µg/ml and 200 µg/ml for 24h and 48h. Representative orthogonal images of OSCC exposed to 200 µg/mL NC-RhoB (H) for 24h (top) and 48h (bottom) acquired in z-stack mode using the Zeiss LSM900 confocal microscope (LD C-Apochromat 40x/1.1 W Korr UV VIS IR), the scale bar indicates 20 µm. Statistical analysis were performed using two-way ANOVA followed either by Dunnett's multiple comparisons test **(A,B,C)** with the according control for each condition, or Tukey's multiple comparisons test **(D,F)**. Data are represented as mean ± SEM. *p < 0,05, **p < 0,005, ***p < 0,001, ****p < 0,0001. *OSCC, oral squamous cell carcinoma cell line (UM-SCC14c); NC, nanocarrier; RhoB, rhodamine-B; Cis, cisplatin; CD, centrifugal dispersion; ND, normal dispersion; WGA, wheat Germ Agglutinin; +, positive control for cell death*.

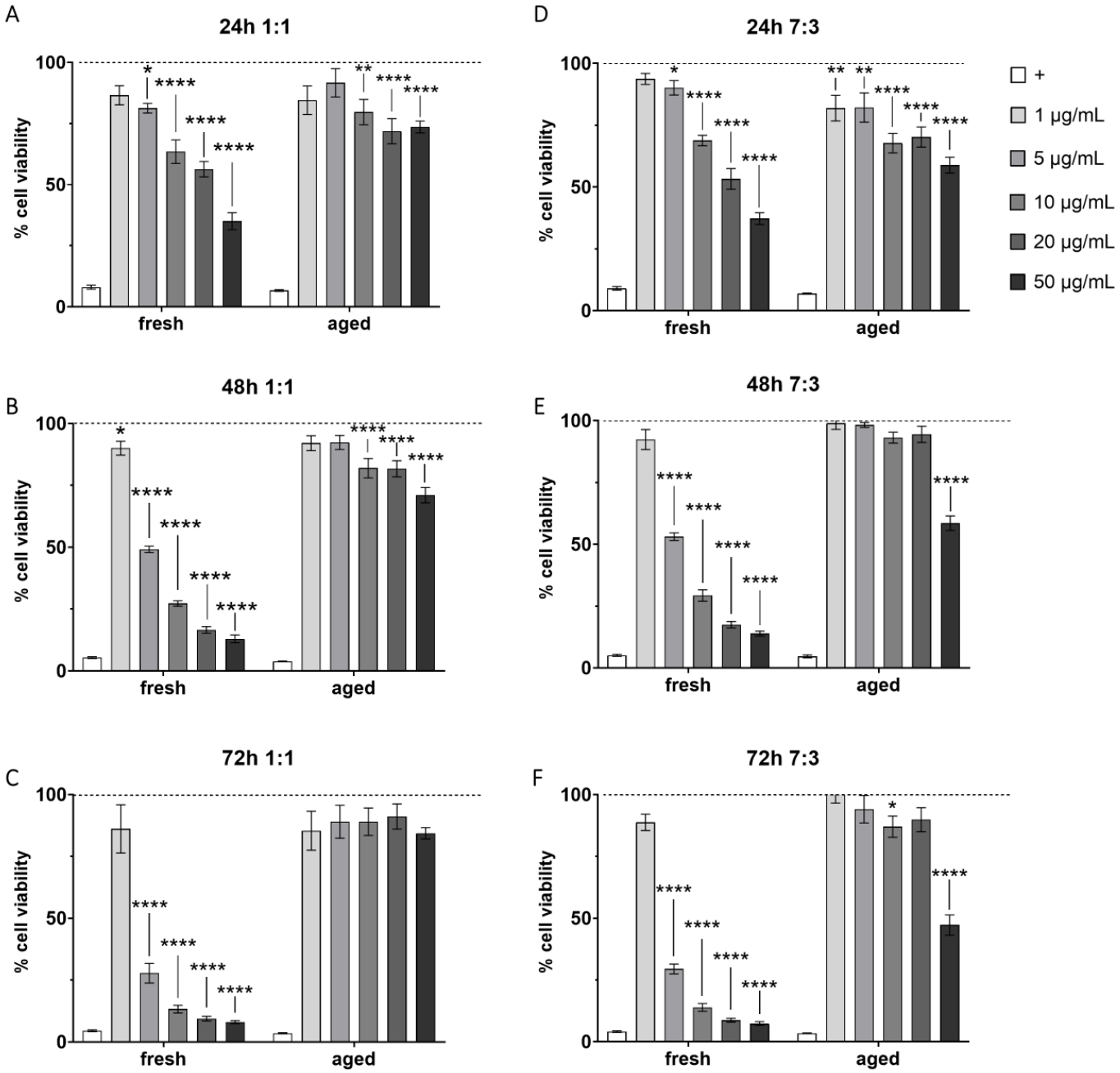

Fig.2 – Cisplatin stability is unaffected by DMSO:H_2O solvent ratios but decreases over time of storage. Cisplatin was dissolved in ratios of 1:1 and 7:3 of DMSO:H_2O solvent mixture and diluted to the indicated concentration range in culture medium. OSCC (n=3) were either treated directly with dissolved cisplatin samples (fresh) or with samples stored for one week in dark surroundings at 4°C (aged). Cell viability was examined using the Alamar Blue assay following 24h, 48h, and 72h of exposure to dissolved cisplatin in 1:1 **(A,B,C)** or 7:3 DMSO:H_2O **(D,E,F)** ratios . Data were normalized to the untreated control (dotted line) and expressed as relative percentages. Data are represented as mean ± SEM. Statistical analysis were performed using two-way ANOVA followed by Dunnett's multiple comparisons test with the according control for each condition. *p < 0,05, **p < 0,005, ***p < 0,001, ****p < 0,0001. *OSCC, oral squamous cell carcinoma cell line (UM-SCC14c); DMSO, dimethylsulfoxide; +, positive control for cell death.*

tBHP induces cytotoxicity in OSCC and HaCaT in a dose-dependent pattern – This second section describes our efforts in investigating the redox status of OSCC to gain further insights in how our designed NCs can be optimized to react to these alterations in redox levels. Initially a positive control for oxidative stress was needed as a reference for the basal conditions. We explored tBHP and H_2O_2 as a positive control, first evaluating the effect of the molecules on cell viability of OSCC (n=3) using an Alamar Blue cell viability assay. While H_2O_2 seemingly has no effect on the viability of OSCC in the given concentrations **(figure 3A)**, treatment with 100µM and 200µM of tBHP resulted in a decrease in viability after 3h and 1h **(figure 3D)** (3h: ***p<0,0001; 1h: *p<0,05; **p<0,005 respectively). Additionally, we tested the effects of H_2O_2 and tBHP on the proliferation of OSCC (n=3) for 24h **(figure3B,E)**. Here, we could observe that H_2O_2 significantly decreased the proliferation of OSCC compared to the control in all conditions, but more pronounced in higher concentrations **(figure 3B)** (10µM: **p<0,005; 100-200 µM: ****p<0,0001), while tBHP significantly reduces proliferation equally across all conditions **(figure 3E)** (****p<0,0001). Following, the effects of these molecules on the viability of a healthy cell control (HaCaTs n=3) was evaluated. HaCaTs showed a decrease in viability following 3h of treatment with H_2O_2 (750-1000 µM: **p< 0,005) **(figure 3C)**. All treatments of tBHP for 3h decreased the viability of HaCaTs compared to the untreated control (****p<0,0001), with a decreasing trend associated with increasing tBHP concentration **(figure 3F)**. These findings indicate that tBHP can serve as a stress-inducer in both OSCC and HaCaT.

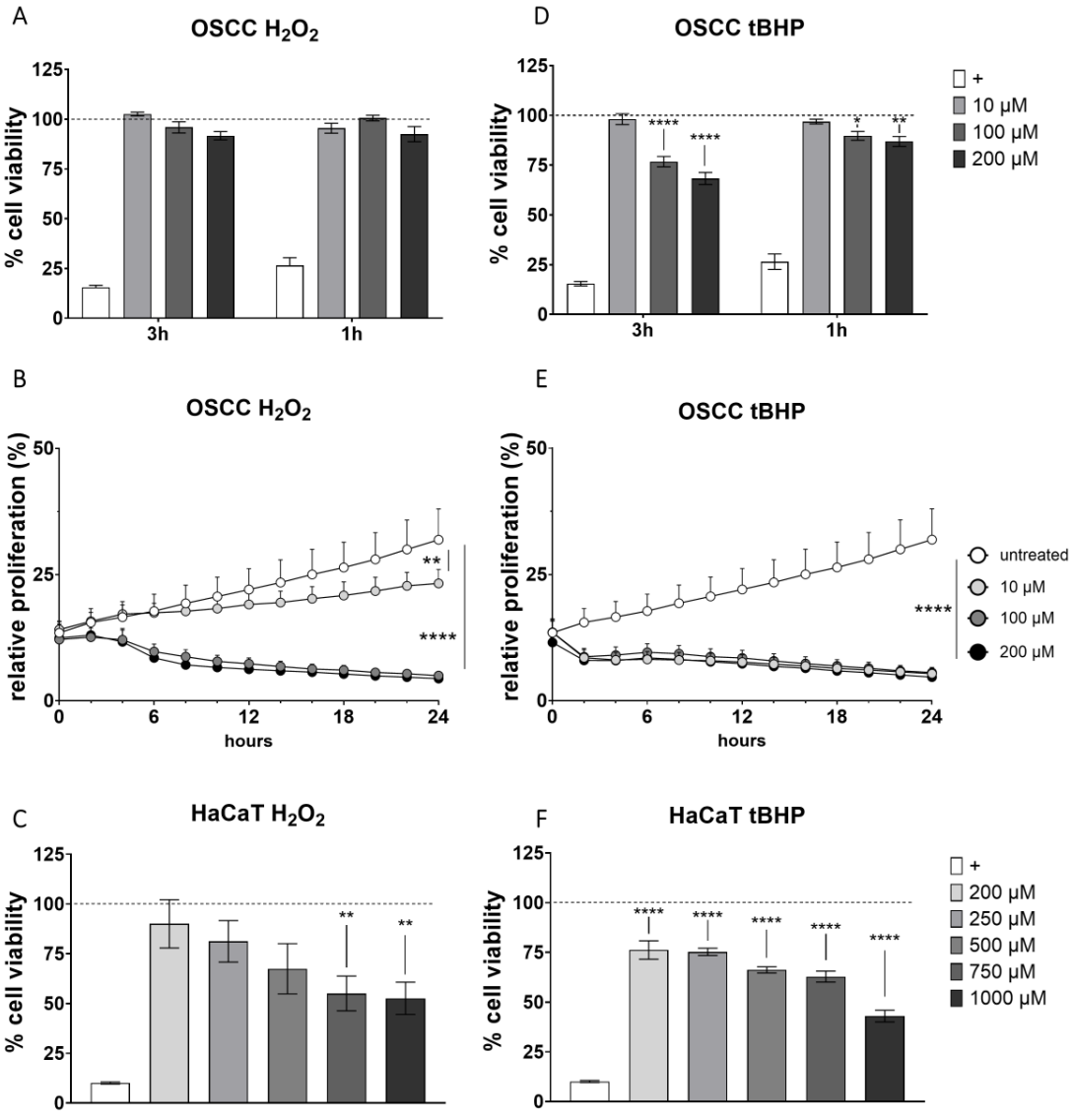

Fig.3 – tBHP is cytotoxic for OSCC and HaCaT in a dose-dependent pattern. To determine the cytotoxic effects of an indicated range of H_2O_2 **(A)** and tBHP **(D)**, OSCC (n=3) were treated followed by Alamar Blue viability assay at 1h and 3h post-treatment. Data were normalized to the untreated control (dotted line) and expressed as relative percentages. To determine the effects on cell proliferation, OSCC (n=3) were exposed to the indicated range of H_2O_2 **(B)** and tBHP **(E)** and monitored at fixed timepoints through live-cell analysis (Incuyte® S3, Sartorius). Data were normalized to the untreated control (white circles) and expressed as relative proliferation, cut off at 24h. As a healthy cell control, HaCaT (n=3) were exposed to the indicated range of H2O2 **(C)** and tBHP **(F)** for 3h followed by Alamar Blue viability assay. Data are represented as mean ± SEM. Statistical analysis was performed using two-way ANOVA followed by Dunnett's multiple comparisons test with the according control for each condition. *p < 0,05, **p < 0,005, ***p < 0,001, ****p < 0,0001. *OSCC, oral squamous cell carcinoma cell line (UM-SCC14c); HaCaT, Human immortalized keratinocyte cell line; tBHP, tert-Butyl hydroperoxide, H_2O_2, hydrogen peroxide; +, positive control for cell death.*

tBHP induces oxidative stress in OSCC – A variety of fluorescent probes were used to detect intracellular ROS and GSH through live-cell imaging on OSCC using tBHP 100 µM as a positive control, as we considered the previous data on viability. As an extra control, we included tBHP 100 µM combined with 1 mM of the ROS-inhibitor NAC. Representative images of the DCFDA, MitoSOX™, and NBD-P probes in **figure 4A-C** visualize the general ROS levels, mitochondrial superoxide generation and the produced GSH levels respectively. The probes were evaluated on untreated, tBHP 100 µM, and tBHP 100 µM + NAC 1 mM treated OSCC (n=2). **(figure 4A-C**, left-to-right respectively). Interestingly, while the DCFDA and NBD-P signals consistently showed a perinuclear localization, the MitoSOX™ dye also colocalized with the nucleus (**figure 4B)**, showing intensely stained regions within the nucleus region. **Figure 4D-F** shows the quantification of OSCC (n=2) for every condition. It was seen that tBHP increased the signal intensity for all probes (*p<0,05; *p<0,05; ****p<0,05 for DCFDA, MitoSOX™, and NBD-P respectively) compared to the untreated control. Interestingly, co-treatment with NAC resulted in a decrease of the NBD-P probe intensity **(figure 4F)** (**p<0,005). Together, these findings indicate that tBHP stimulates the production of ROS and GSH in OSCC. However, experiment repetition is required to conclusively state these findings.

NAC reduces the quantity of oxidative stress generated through tBHP in OSCC – To further evaluate the redox status, flow cytometry experiments were performed using the same treatment conditions on OSCC as previously described. We also included NAC as a single treatment condition to observe if any changes in ROS can be related directly to this molecule. **Figure 5A** shows the quantification of DCFDA+stained OSCC (n=3) as a percentage of each treatment group total. Both tBHP 100 µM alone and in combination with NAC 1mM show an increased proportion of DCFDA+ OSCC compared to the untreated and NAC 1mM single treatment conditions (***p<0,001). Similar trends are observed for the MitoSOX+ OSCC (n=1) **(figure 5B)** and NBD-P+ OSCC (n=1) **(figure 5C),** which will have to be confirmed through sufficient repetitions. The representative histogram depicting DCFDA signal **(Figure 5D)** indicates a shift in fluorescence intensity following tBHP treatment compared to the other conditions, which was not observed for the remaining probes **(figure 5E,F)**. When evaluating the DCFDA fluorescence intensity through microplate assays, OSCC (n=3) treated with tBHP 100µM for 3h resulted in a significant increase compared to the other treatments **(figure 5G)** (****p<0,0001). The fluorescence intensity readings from the MitoSOX™ ,NBD-P, and other redox probes provided poor signal when using the microplate reader (**figure S3)**. Together these findings indicate that NAC can decrease the DCFDA+ signal generated through tBHP in OSCC and thus can serve as a control treatment to scavenge ROS in OSCC.

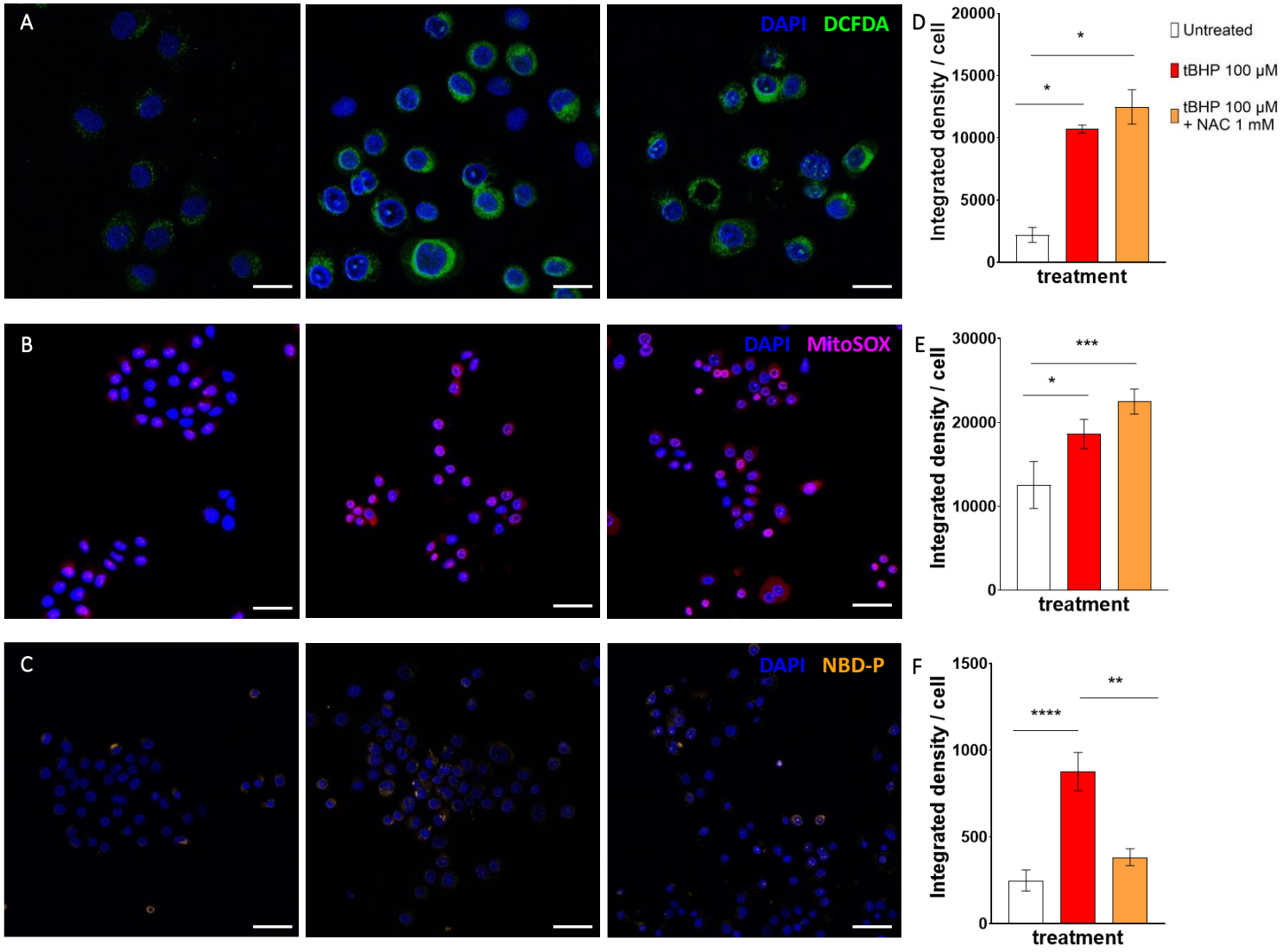

Fig.4 – tBHP induces oxidative stress in OSCC. A variety of fluorescent probes were used to detect intracellular ROS and GSH through live-cell imaging (Zeiss LSM880, 37°C, 5% CO2) of OSCC (n=2) following 3h treatment with either tBHP 100 µM by itself or in combination with the ROS inhibitor NAC 1 mM. A signal intensity threshold was manually determined for each fluorescent probe and kept consistent across all experimental conditions. Area, mean fluorescence intensity and cell count were measured and the integrated density per cell was determined **(D,E,F)**. Data are represented as mean ± SEM. Representative images (Plan-Apochromat 20x/0.8 M27) of OSCC exposed to culture medium, tBHP 100 µM, and tBHP 100 µM in combination with NAC 1 mM in respective left to right order, visualized using ROS detection probes DCFDA **(A)**, MitoSOX™ **(B)**, and GSH-reporting probe NBD-P **(C)**. The scalebar indicates 50 µm across all conditions. Statistical analysis was performed using one-way ANOVA followed by Tukey's multiple comparison test. *p < 0,05, **p < 0,005, ***p < 0,001, ****p < 0,0001. *OSCC, oral squamous cell carcinoma cell line (UM-SCC14c) ;DCFDA, 2',7'-dichlorofluorescin diacetate; MitoSOX™, mitochondrial superoxide probe ; NBD-P,GSH-specific on-off fluorescent probe; tBHP, tert-butyl hydroperoxide; NAC, N-acetyl-L-cysteine.*

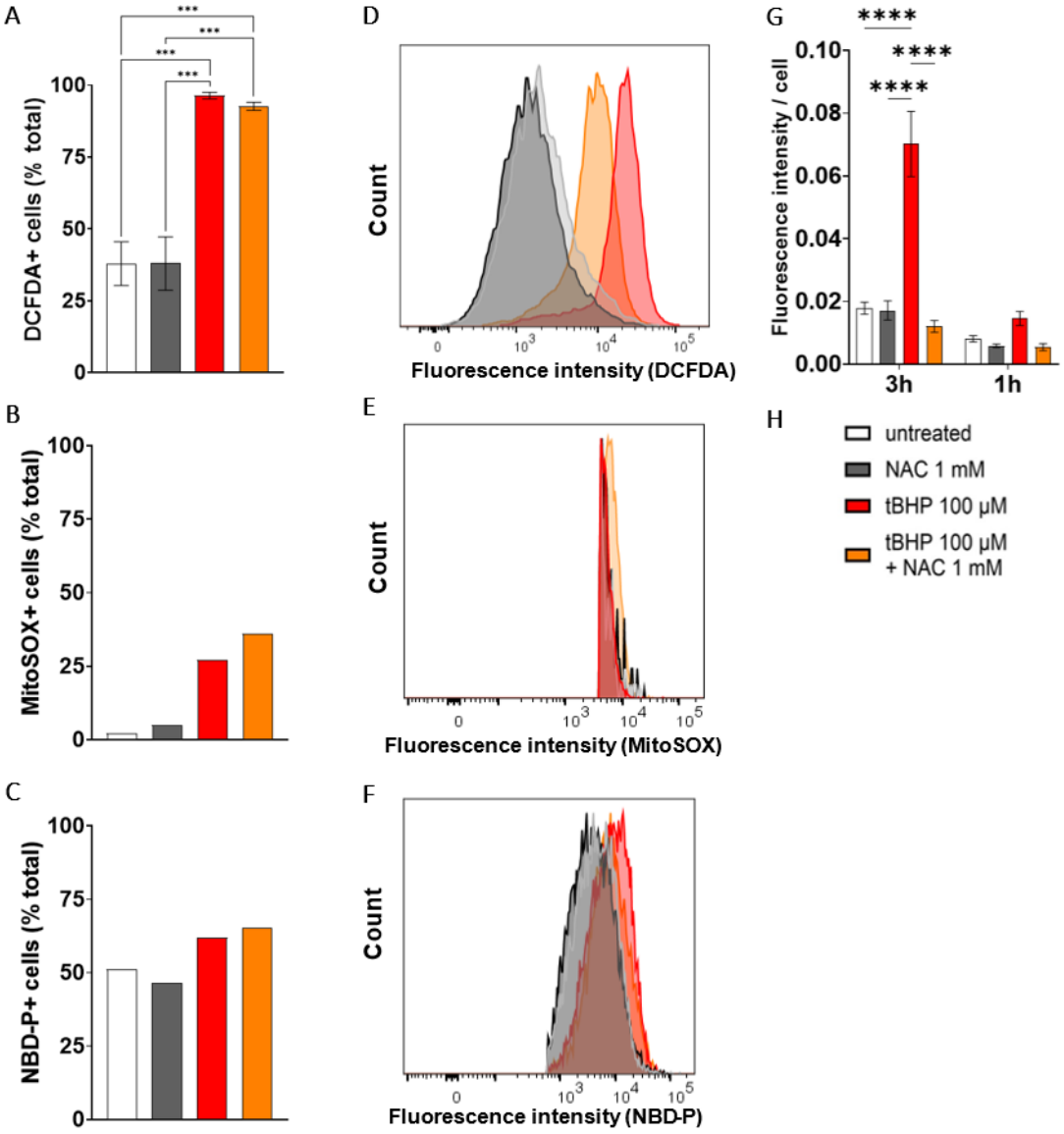

Fig.5 – NAC reduces the quantity of oxidative stress generated through tBHP in OSCC. Oxidative stress was assessed through flow cytometry (LSRFortessa, BD Biosciences) of OSCC following 3h treatment with either tBHP 100 µM by itself or in combination with the ROS inhibitor NAC 1 mM. Following gating steps, the percentage of total events per condition was determined for the DCFDA (n=3) **(A)**, MitoSOX (n=1) **(B)**, and NBD-P (n=1) **(C)** probes. Representative histograms highlighting the shift in fluorescent intensity of DCFDA **(D)**, MitoSOX **(E)**, and NBD-P **(F)** probes across the treatment conditions. **(G)** Microplate assay showing ROS detection through DCFDA probe in OSCC (n=3) treated as described for 3h and 1h. **(H)** figure legend indicating the treatment conditions across all experiments. Data are represented as mean ± SEM. Statistical analysis was performed using one-way ANOVA, followed by Tukey's multiple comparisons test. ***p < 0,001, ****p < 0,0001. *OSCC, oral squamous cell carcinoma cell line (UM-SCC14c); DCFDA, 2',7'-dichlorofluorescin diacetate; MitoSOX™ , mitochondrial superoxide probe; NBD-P,GSH-specific on-off fluorescent probe; tBHP, tert-butyl hydroperoxide; NAC, N-acetyl-L-cysteine.*

DISCUSSION

The main goal of this study was to design and optimize ROS-responsive NCs with the ability to deliver cisplatin to OSCC *in vitro* and thereby induce apoptosis. So far we have shown that the NCs are successful in delivering cargo to the target cells, and that cargo is internalized. However, no notable cytotoxic effects were seen following treatment with these NCs. This finding suggests that the drug loading content of cisplatin in our current NCs is insufficiently high in order to elicit cytotoxic effects. Therefore, current efforts will focus on the optimization of the synthesis process which would allow to increase the drug loading content, and thereby also the therapeutic potential. Secondly, we investigated the presence of ROS and GSH in the OSCC through a range of fluorescent probes. We established a positive control for the generation of ROS signal using tBHP, and proved that this signal is reduced through a combined treatment with the ROS-inhibitor NAC. Our results suggest that the generalized oxidative stress probe DCFDA provides the most consistent readouts for OSCC *in vitro*. Other probes, including the specific mitochondrial superoxide probe MitoSOX, and the GSH-sensing probe NBD-P show promising first results but will require repeated testing to ensure functionality in OSCC.

Nanocarrier optimization – When evaluating the cellular uptake properties of our designed NCs through confocal Z-stack imaging, we indicated a predominant localization at the perinuclear region, suggesting the NCs are internalized. This internalization may be mediated through a variety of active uptake mechanisms, followed by intracellular trafficking to other subcellular locations (35). Since the NCs are designed to react with ROS, the localization around the nucleus suggests that this region shows elevations of oxidative stress, which may contribute to the accumulation of DNA damage and dysregulation of signaling pathways seen in cancer (36, 37). By evaluating the viability effects of our designed NCs on OSCC, we could observe that the cell viability signal increased following 24h of exposure, while the signal was stable or decreased in the 48h conditions. This finding could be explained through an increase in metabolic activity following the initial exposure of OSCC to the NCs. The NCs may interact with mitochondrial respiration, thereby increasing activity as seen in other types of nano-sized particles (38). This increased activity can in turn increase the amount of converted resazurin dye of the Alamar Blue assay, and as a consequence, also the viability signal readout. The stable signal following 48h of exposure suggests that this timepoint is more indicative of the cytotoxic effects of the NCs, as the metabolic activity returned to normal levels. Since our NCs are composed of a biopolymer, they offer the advantage of increased biocompatibility over other types of shell materials (39, 40), as indicated by our results. However, in the 48h conditions, it was shown that the highest concentration of both cisplatin- and rhodamine-b loaded NCs decreased OSCC viability. Since no differences were seen between the cisplatin and rhodamine-b cargo NCs, this finding can be attributed to a possible cytotoxic effect of the NC materials itself at high concentrations, irrespective of the cargo content, leading to a low therapeutic range (40). To increase this range, we would have to increase the drug-loading content, thereby reducing the total amount of NCs having to be administered to reach therapeutic effects of cisplatin. Ongoing research efforts explore a variety of fabrication strategies to achieve high-drug loading content, which proves a challenge across multiple NC platforms (41). In a similar application to ours, Badparvar et al. have provided substantial evidence for the use of their organic redox-responsive NCs loaded with docetaxel to combat breast cancer (42). Their platform is based on disulfide-containing hyperbranched methyloxide-polyethylene-glycol polymeric NCs that respond to low extracellular pH and high GSH, loaded with docetaxel dissolved in DMSO. Using this method, the researchers state that their NCs show a remarkably high drug-loading capacity at a 10:1 ratio of NC to drug (42). Due to the poor water solubility of cisplatin (1 mg/mL), we also considered DMSO as a solvent for our NCs in an attempt to increase the drug-loading capacity. We initially examined the stability of cisplatin in a ratio of 1:1 and 7:3 DMSO to H_2O and noticed a decrease in effectivity following one week of sample storage. A study performed by Hall et al. showed that DMSO changes the structure of the cisplatin molecules and displaces the chloride ligands, thereby inhibiting their cytotoxic effect, which would explain our findings (43). Instead of DMSO, Hall et al. propose using other organic solvents like dimethylformamide (DMF), as this would not affect cisplatin stability, as supported by a study performed by Yi et al. (44). Besides considering the solvent for cisplatin, alterations to

the production process and optimization of NC properties including size, morphology, and chemical modifications to increase drug-polymer interactions all could contribute to an increased drug-loading capacity for our NC platform (39, 41). Once optimized *in vitro*, the NCs can be assessed for their biodistribution properties and efficacy on in house *in vivo* models of OSCC. These models are based on the administration of the carcinogen 4-nitroquinoline 1-oxide (4NQO) through drinking water and the xenografting of OSCC in immunosuppressed mice, each having their own advantages in evaluating treatment efficiency (45, 46). Taken together, multiple factors have to be carefully considered in the ongoing process of our NCs optimization and future *in vivo* testing. Unfortunately, we were unable to achieve this in the duration of the thesis project due to time constraints.

Investigating the redox status in OSCC – In a parallel approach to improving our NCs, we sought to further understand the complex redox balance within the tumor microenvironment (TME) through mapping ROS and GSH using fluorescent probes. In order to test the ROS and GSH levels, we explored both the use of hydrogen peroxide (H_2O_2) and tert-butyl hydroperoxide (tBHP) as a positive control for the induction of oxidative stress in OSCC and HaCaT cell lines. The finding that H_2O_2 has a less pronounced effect on both OSCC and HaCaT cell cytotoxicity compared to tBHP can be explained through the presence of catalase enzymes which degrade the added H_2O_2 as discussed by Ransy et al. (47). Their study indicates that cells neutralize H_2O_2 within a few minutes, therefore requiring high concentrations to see effects, as supported by our findings. Contrastingly, tBHP is shown to induce oxidative stress through a variety of mechanisms, including the depletion of antioxidant defences (48, 49). Notably, we found HaCaTs to require higher doses of tBHP to observe an effect, compared to OSCC. This finding could be supported by the inherent dysregulation of the redox system in cancer cells as one of the hallmarks driving cancer proliferation (50). Levels of ROS are also seen to be elevated in OSCC (51), and therefore these cells would be more sensitive to external ROS inducing agents like tBHP. Using tBHP as a positive control for oxidative stress, we observed the most consistent results using the general ROS indicator DCFDA. We have shown that ROS levels increase following tBHP administration, and that co-administration of the ROS-inhibitor NAC reduces these levels. This finding can be explained through the antioxidant effects of NAC, which is hypothesized to act through triggering intracellular H_2S production, thereby providing cells with cytoprotective effects (52). Together this provides us with control treatments for the evaluation of the redox status in OSCC through the use of other general and specific ROS probes *in vitro* before considering applications *in vivo*. Besides DCFDA, the specific mitochondrial superoxide MitoSOX and GSH-sensing NBD-P probes showed promising first results *in vitro,* but due to time constraints we were unable to repeat the experiments to a sufficient replicate number in order to make a conclusive statement. Future repetitions will have to point out if these probes prove useful for our application. Alternative to these probes, we could further explore the redox status through other kits including Thioltracker, CellROX, and Peroxy Orange 1. Surprisingly we noticed the mitochondrial superoxide probe MitoSOX to colocalize with the nucleus, suggesting presence of superoxide in this cellular structure. This finding may indicate that the cells may be apoptotic, as mitochondrial superoxide generation has previously been linked to apoptotic markers in other cell types (53). It is possible that the superoxide generated in mitochondria can translocate to the nucleus under cellular stress. This is supported by other research, which has shown that the antioxidant enzyme superoxide dismutase 1 relocates to the nucleus in response to oxidative stress, thereby attempting to guard the genome from oxidative damage (54). Our findings also indicate through the NBD-P probe that intracellular reduced GSH levels are increased in oxidative stress. This is an expected finding, as GSH is an important regulator of the cellular redox state, providing protective effects by reducing ROS, thereby neutralizing their harmful effects (25). Kwon et al. demonstrated that exogenous administration of GSH protects cells from oxidative stress-induced damage and apoptosis, further highlighting its antioxidant effects (55). In other research performed by Zhang et al., the NBD-P probe has already been evaluated *in vivo,* providing good results in their renal cell carcinoma mouse model, using the IVIS Spectrum bioluminescence system (33). Using the same imaging system, the peroxy-caged luciferin-1 (PCL-1) is a useful probe that upon oxidation forms luciferin which can be used in luciferase systems to generate light (56). Towards this end, we have successfully

transduced our OSCC cell line as described in the methods section, and are conducting *in vitro* testing of the probe. Alternatively, researchers are exploring methods based on positron-emission tomography, using radioactively labelled probes to detect ROS *in vivo* (57), or methods making use of electron paramagnetic resonance (EPR) (58). These methods are promising, but remain a challenge due to the short lived and rapidly changing nature of ROS, complicating the practical aspects (59). Finally, methods of measuring oxidative damage can be considered to overcome the practical difficulties of measuring ROS directly. Oxidative stress can be derived from damage to lipids, proteins, and nucleic acids which can serve as biomarkers for oxidative damage (59).

CONCLUSION

This work summarizes the current state of the project, highlighting the need for optimization of the NCs to increase drug-loading capacity, and further exploration of ROS and GSH signals to better target the NCs for the elevated oxidative stress levels in the TME. Analogous to Badparvar et al. targeting both pH and GSH signals, we intend to implement a 'dual-shell' principle that is capable of reacting both to ROS and GSH, thereby increasing the sensitivity of the NCs to the OSCC specifically. Once the NCs are optimized, they can be assessed using our in-house *in vivo* models of OSCC. The optimized NCs are expected to reduce off-target effects compared to systemic cisplatin administration, while also maintaining biocompatibility. Taken together, our NCs would provide an alternative treatment sparing HNSCC patients from severe side-effects associated with current therapeutic options.

REFERENCES

1. Sung H, Ferlay J, Siegel RL, Laversanne M, Soerjomataram I, Jemal A, et al. Global Cancer Statistics 2020: GLOBOCAN Estimates of Incidence and Mortality Worldwide for 36 Cancers in 185 Countries. CA Cancer J Clin. 2021;71(3):209-49.
2. Chow LQM. Head and Neck Cancer. New England Journal of Medicine. 2020;382(1):60-72.
3. Gormley M, Creaney G, Schache A, Ingarfield K, Conway DI. Reviewing the epidemiology of head and neck cancer: definitions, trends and risk factors. British Dental Journal. 2022;233(9):780-6.
4. Johnson DE, Burtness B, Leemans CR, Lui VWY, Bauman JE, Grandis JR. Head and neck squamous cell carcinoma. Nature Reviews Disease Primers. 2020;6(1):92.
5. Barsouk A, Aluru JS, Rawla P, Saginala K, Barsouk A. Epidemiology, Risk Factors, and Prevention of Head and Neck Squamous Cell Carcinoma. Med Sci (Basel). 2023;11(2).
6. Canning M, Guo G, Yu M, Myint C, Groves MW, Byrd JK, et al. Heterogeneity of the Head and Neck Squamous Cell Carcinoma Immune Landscape and Its Impact on Immunotherapy. Front Cell Dev Biol. 2019;7:52.
7. Yousem DM, Gad K, Tufano RP. Resectability issues with head and neck cancer. AJNR Am J Neuroradiol. 2006;27(10):2024-36.
8. Avan A, Postma TJ, Ceresa C, Avan A, Cavaletti G, Giovannetti E, et al. Platinum-induced neurotoxicity and preventive strategies: past, present, and future. Oncologist. 2015;20(4):411-32.
9. Barabas K, Milner R, Lurie D, Adin C. Cisplatin: a review of toxicities and therapeutic applications. Vet Comp Oncol. 2008;6(1):1-18.
10. Miller RP, Tadagavadi RK, Ramesh G, Reeves WB. Mechanisms of Cisplatin nephrotoxicity. Toxins (Basel). 2010;2(11):2490-518.
11. Tang C, Livingston MJ, Safirstein R, Dong Z. Cisplatin nephrotoxicity: new insights and therapeutic implications. Nature Reviews Nephrology. 2023;19(1):53-72.
12. Alghamdi MA, Fallica AN, Virzì N, Kesharwani P, Pittalà V, Greish K. The Promise of Nanotechnology in Personalized Medicine. J Pers Med. 2022;12(5).
13. Kenchegowda M, Rahamathulla M, Hani U, Begum MY, Guruswamy S, Osmani RAM, et al. Smart Nanocarriers as an Emerging Platform for Cancer Therapy: A Review. Molecules. 2021;27(1).
14. Fan D, Cao Y, Cao M, Wang Y, Cao Y, Gong T. Nanomedicine in cancer therapy. Signal Transduction and Targeted Therapy. 2023;8(1):293.
15. Sabit H, Abdel-Hakeem M, Shoala T, Abdel-Ghany S, Abdel-Latif MM, Almulhim J, et al. Nanocarriers: A Reliable Tool for the Delivery of Anticancer Drugs. Pharmaceutics. 2022;14(8).
16. Wu J. The Enhanced Permeability and Retention (EPR) Effect: The Significance of the Concept and Methods to Enhance Its Application. J Pers Med. 2021;11(8).
17. Golombek SK, May JN, Theek B, Appold L, Drude N, Kiessling F, et al. Tumor targeting via EPR: Strategies to enhance patient responses. Adv Drug Deliv Rev. 2018;130:17-38.
18. Raza A, Rasheed T, Nabeel F, Hayat U, Bilal M, Iqbal HMN. Endogenous and Exogenous Stimuli-Responsive Drug Delivery Systems for Programmed Site-Specific Release. Molecules. 2019;24(6).
19. AlSawaftah NM, Awad NS, Pitt WG, Husseini GA. pH-Responsive Nanocarriers in Cancer Therapy. Polymers (Basel). 2022;14(5).
20. Curry JM, Sprandio J, Cognetti D, Luginbuhl A, Bar-ad V, Pribitkin E, et al. Tumor microenvironment in head and neck squamous cell carcinoma. Semin Oncol. 2014;41(2):217-34.
21. Weinberg F, Ramnath N, Nagrath D. Reactive Oxygen Species in the Tumor Microenvironment: An Overview. Cancers (Basel). 2019;11(8).
22. Chandel NS, Maltepe E, Goldwasser E, Mathieu CE, Simon MC, Schumacker PT. Mitochondrial reactive oxygen species trigger hypoxia-induced transcription. Proc Natl Acad Sci U S A. 1998;95(20):11715-20.
23. Costa A, Scholer-Dahirel A, Mechta-Grigoriou F. The role of reactive oxygen species and metabolism on cancer cells and their microenvironment. Semin Cancer Biol. 2014;25:23-32.
24. Schafer ZT, Grassian AR, Song L, Jiang Z, Gerhart-Hines Z, Irie HY, et al. Antioxidant and oncogene rescue of metabolic defects caused by loss of matrix attachment. Nature. 2009;461(7260):109-13.
25. Kennedy L, Sandhu JK, Harper ME, Cuperlovic-Culf M. Role of Glutathione in Cancer: From Mechanisms to Therapies. Biomolecules. 2020;10(10).

26. Ling X, Zhang S, Shao P, Wang P, Ma X, Bai M. Synthesis of a reactive oxygen species responsive heterobifunctional thioketal linker. Tetrahedron Lett. 2015;56(37):5242-4.
27. Liu B, Thayumanavan S. Mechanistic Investigation on Oxidative Degradation of ROS-Responsive Thioacetal/Thioketal Moieties and Their Implications. Cell Reports Physical Science. 2020;1(12):100271.
28. Chen D, Zhang G, Li R, Guan M, Wang X, Zou T, et al. Biodegradable, Hydrogen Peroxide, and Glutathione Dual Responsive Nanoparticles for Potential Programmable Paclitaxel Release. Journal of the American Chemical Society. 2018;140(24):7373-6.
29. Wilson DS, Dalmasso G, Wang L, Sitaraman SV, Merlin D, Murthy N. Orally delivered thioketal nanoparticles loaded with TNF-α-siRNA target inflammation and inhibit gene expression in the intestines. Nat Mater. 2010;9(11):923-8.
30. Rinaldi A, Caraffi R, Grazioli MV, Oddone N, Giardino L, Tosi G, et al. Applications of the ROS-Responsive Thioketal Linker for the Production of Smart Nanomedicines. Polymers (Basel). 2022;14(4).
31. Capek I. On inverse miniemulsion polymerization of conventional water-soluble monomers. Adv Colloid Interface Sci. 2010;156(1-2):35-61.
32. Tiscornia G, Singer O, Verma IM. Production and purification of lentiviral vectors. Nat Protoc. 2006;1(1):241-5.
33. Zhang C, Qin Y, Deng C, Zhu N, Shi Y, Wang W, et al. GSH-specific fluorescent probe for sensing, bioimaging, rapid screening of natural inhibitor Celastrol and ccRCC theranostics. Anal Chim Acta. 2023;1248:340933.
34. Ng N, Ooi L. A Simple Microplate Assay for Reactive Oxygen Species Generation and Rapid Cellular Protein Normalization. Bio-protocol. 2021;11(1):e3877.
35. Behzadi S, Serpooshan V, Tao W, Hamaly MA, Alkawareek MY, Dreaden EC, et al. Cellular uptake of nanoparticles: journey inside the cell. Chem Soc Rev. 2017;46(14):4218-44.
36. Klaunig JE, Wang Z. Oxidative stress in carcinogenesis. Current Opinion in Toxicology. 2018;7:116-21.
37. Iqbal MJ, Kabeer A, Abbas Z, Siddiqui HA, Calina D, Sharifi-Rad J, et al. Interplay of oxidative stress, cellular communication and signaling pathways in cancer. Cell Communication and Signaling. 2024;22(1):7.
38. Manke A, Wang L, Rojanasakul Y. Mechanisms of nanoparticle-induced oxidative stress and toxicity. Biomed Res Int. 2013;2013:942916.
39. Jia L, Zhang P, Sun H, Dai Y, Liang S, Bai X, et al. Optimization of Nanoparticles for Smart Drug Delivery: A Review. Nanomaterials (Basel). 2021;11(11).
40. Egbuna C, Parmar VK, Jeevanandam J, Ezzat SM, Patrick-Iwuanyanwu KC, Adetunji CO, et al. Toxicity of Nanoparticles in Biomedical Application: Nanotoxicology. J Toxicol. 2021;2021:9954443.
41. Shen S, Wu Y, Liu Y, Wu D. High drug-loading nanomedicines: progress, current status, and prospects. Int J Nanomedicine. 2017;12:4085-109.
42. Badparvar F, Marjani AP, Salehi R, Ramezani F. Dual pH/redox-responsive hyperbranched polymeric nanocarriers with TME-trigger size shrinkage and charge reversible ability for amplified chemotherapy of breast cancer. Scientific Reports. 2024;14(1):8567.
43. Hall MD, Telma KA, Chang KE, Lee TD, Madigan JP, Lloyd JR, et al. Say no to DMSO: dimethylsulfoxide inactivates cisplatin, carboplatin, and other platinum complexes. Cancer Res. 2014;74(14):3913-22.
44. Yi YW, Bae I. Effects of solvents on in vitro potencies of platinum compounds. DNA Repair (Amst). 2011;10(11):1084-5.
45. Sano D, Myers JN. Xenograft models of head and neck cancers. Head Neck Oncol. 2009;1:32.
46. Sagheer SH, Whitaker-Menezes D, Han JYS, Curry JM, Martinez-Outschoorn U, Philp NJ. 4NQO induced carcinogenesis: A mouse model for oral squamous cell carcinoma. Methods Cell Biol. 2021;163:93-111.
47. Ransy C, Vaz C, Lombès A, Bouillaud F. Use of H(2)O(2) to Cause Oxidative Stress, the Catalase Issue. Int J Mol Sci. 2020;21(23).
48. Davies MJ. Detection of peroxyl and alkoxyl radicals produced by reaction of hydroperoxides with rat liver microsomal fractions. Biochemical Journal. 1989;257(2):603-6.

49. CRANE D, HÄUSSINGER D, GRAF P, SIES H. Decreased Flux through Pyruvate Dehydrogenase by Thiol Oxidation during t-Butyl Hydroperoxide Metabolism in Perfused Rat Liver. Biological Chemistry. 1983;364(2):977-88.
50. Xing F, Hu Q, Qin Y, Xu J, Zhang B, Yu X, et al. The Relationship of Redox With Hallmarks of Cancer: The Importance of Homeostasis and Context. Front Oncol. 2022;12:862743.
51. Manjunathan R, Jayaraman S, S R, Ileng Kumaran R, Chandrakesan P, Rajagopal P, et al. Reactive Oxygen Species in Oral Squamous Cell Carcinoma Progression and Importance of Stem Cells in Cancer Therapeutics. In: Chakraborti S, editor. Handbook of Oxidative Stress in Cancer: Therapeutic Aspects. Singapore: Springer Singapore; 2021. p. 1-24.
52. Ezeriņa D, Takano Y, Hanaoka K, Urano Y, Dick TP. N-Acetyl Cysteine Functions as a Fast-Acting Antioxidant by Triggering Intracellular H(2)S and Sulfane Sulfur Production. Cell Chem Biol. 2018;25(4):447-59.e4.
53. Mukhopadhyay P, Rajesh M, Haskó G, Hawkins BJ, Madesh M, Pacher P. Simultaneous detection of apoptosis and mitochondrial superoxide production in live cells by flow cytometry and confocal microscopy. Nat Protoc. 2007;2(9):2295-301.
54. Tsang CK, Liu Y, Thomas J, Zhang Y, Zheng XFS. Superoxide dismutase 1 acts as a nuclear transcription factor to regulate oxidative stress resistance. Nature Communications. 2014;5(1):3446.
55. Kwon DH, Cha HJ, Lee H, Hong SH, Park C, Park SH, et al. Protective Effect of Glutathione against Oxidative Stress-induced Cytotoxicity in RAW 264.7 Macrophages through Activating the Nuclear Factor Erythroid 2-Related Factor-2/Heme Oxygenase-1 Pathway. Antioxidants (Basel). 2019;8(4).
56. Zielonka J, Podsiadły R, Zielonka M, Hardy M, Kalyanaraman B. On the use of peroxy-caged luciferin (PCL-1) probe for bioluminescent detection of inflammatory oxidants in vitro and in vivo - Identification of reaction intermediates and oxidant-specific minor products. Free Radic Biol Med. 2016;99:32-42.
57. Boutagy NE, Wu J, Cai Z, Zhang W, Booth CJ, Kyriakides TC, et al. In Vivo Reactive Oxygen Species Detection With a Novel Positron Emission Tomography Tracer, (18)F-DHMT, Allows for Early Detection of Anthracycline-Induced Cardiotoxicity in Rodents. JACC Basic Transl Sci. 2018;3(3):378-90.
58. Dikalov SI, Polienko YF, Kirilyuk I. Electron Paramagnetic Resonance Measurements of Reactive Oxygen Species by Cyclic Hydroxylamine Spin Probes. Antioxid Redox Signal. 2018;28(15):1433-43.
59. Murphy MP, Bayir H, Belousov V, Chang CJ, Davies KJA, Davies MJ, et al. Guidelines for measuring reactive oxygen species and oxidative damage in cells and in vivo. Nature Metabolism. 2022;4(6):651-62.

Acknowledgements – Q.C. is grateful for the supervision and feedback N.C. provided during the internship. Prof. Dr. Karen Smeets is thanked for providing access to the LSM 880 confocal microscope. The Advanced Optical Microscopy Centre (AOMC) is thanked for providing access to the LSM 900 live-cell confocal microscope. Nele Theysmans and prof. Wouter Maes (Design & Synthesis of Organic Semiconductors (DSOS), Materials Chemistry (MATCHEM)) are thanked for the synthesis of NBD-P and PCL-1 probes.

Author contributions – N.C. and E.W. conceived and designed the research. S.N. and A.E. designed the nanocarriers. S.N. synthesized and evaluated the physicochemical properties of the nanocarriers. Q.C. and N.C. performed the experiments. Q.C. performed data analysis and wrote the thesis. Q.C. and N.C. carefully edited the manuscript.

SUPPLEMENTARY

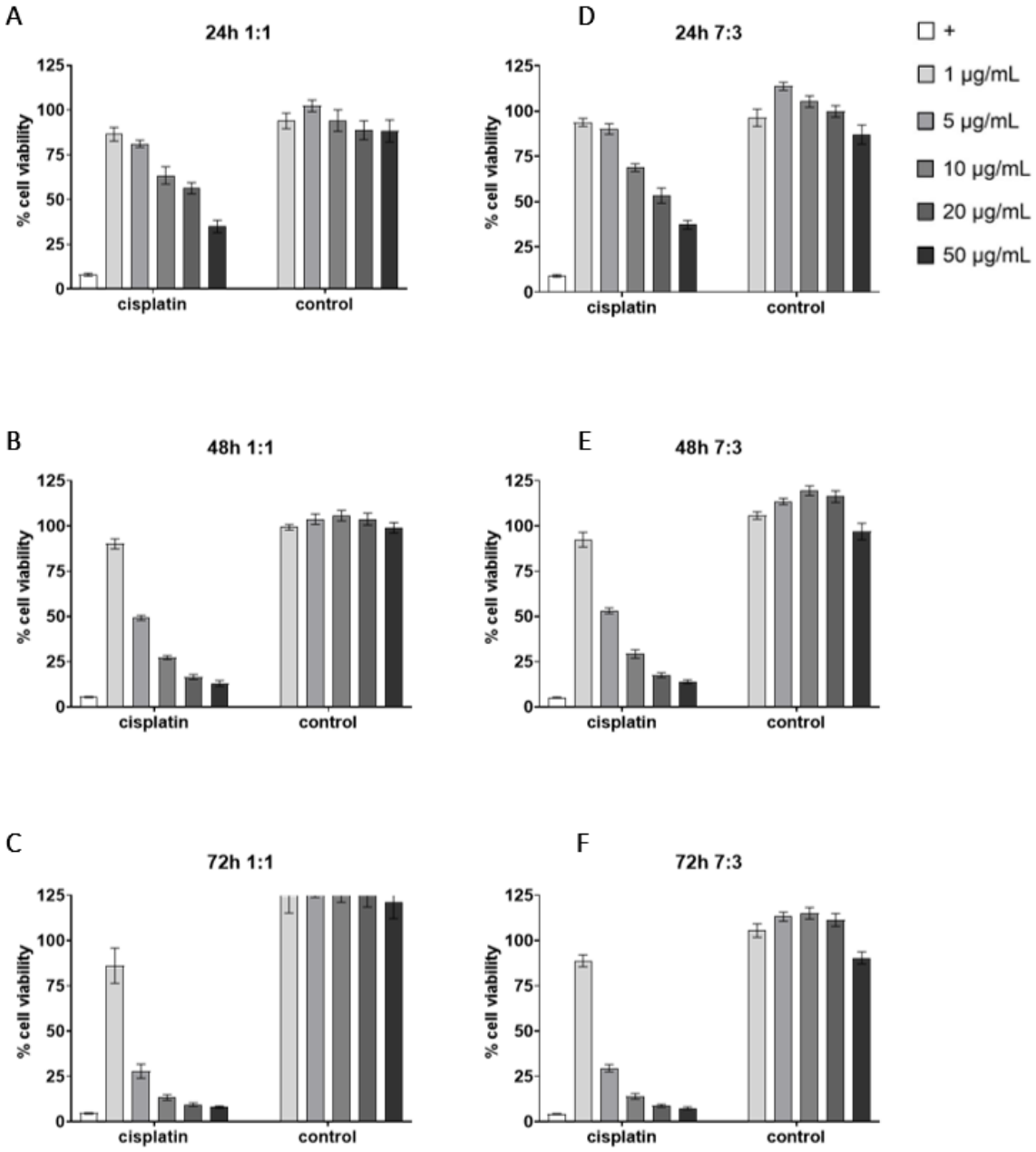

Fig. S1 – The effect of fresh cisplatin samples compared to vehicle control. Cisplatin was dissolved in ratios of 1:1 and 7:3 of DMSO:H_2O solvent mixture and diluted to the indicated concentration range in culture medium. OSCC (n=3) were treated either with fresh dissolved cisplatin samples or the solvent vehicle (control). Cell viability was examined using the Alamar Blue assay following 24h, 48h, and 72h of exposure to dissolved cisplatin or vehicle in 1:1 **(A,B,C)** or 7:3 **(D,E,F)** ratios . Data were normalized to the untreated control and expressed as relative percentages. Data are represented as mean ± SEM. *OSCC, oral squamous cell carcinoma cell line (UM-SCC14c); DMSO, dimethylsulfoxide; +, positive control for cell death.*

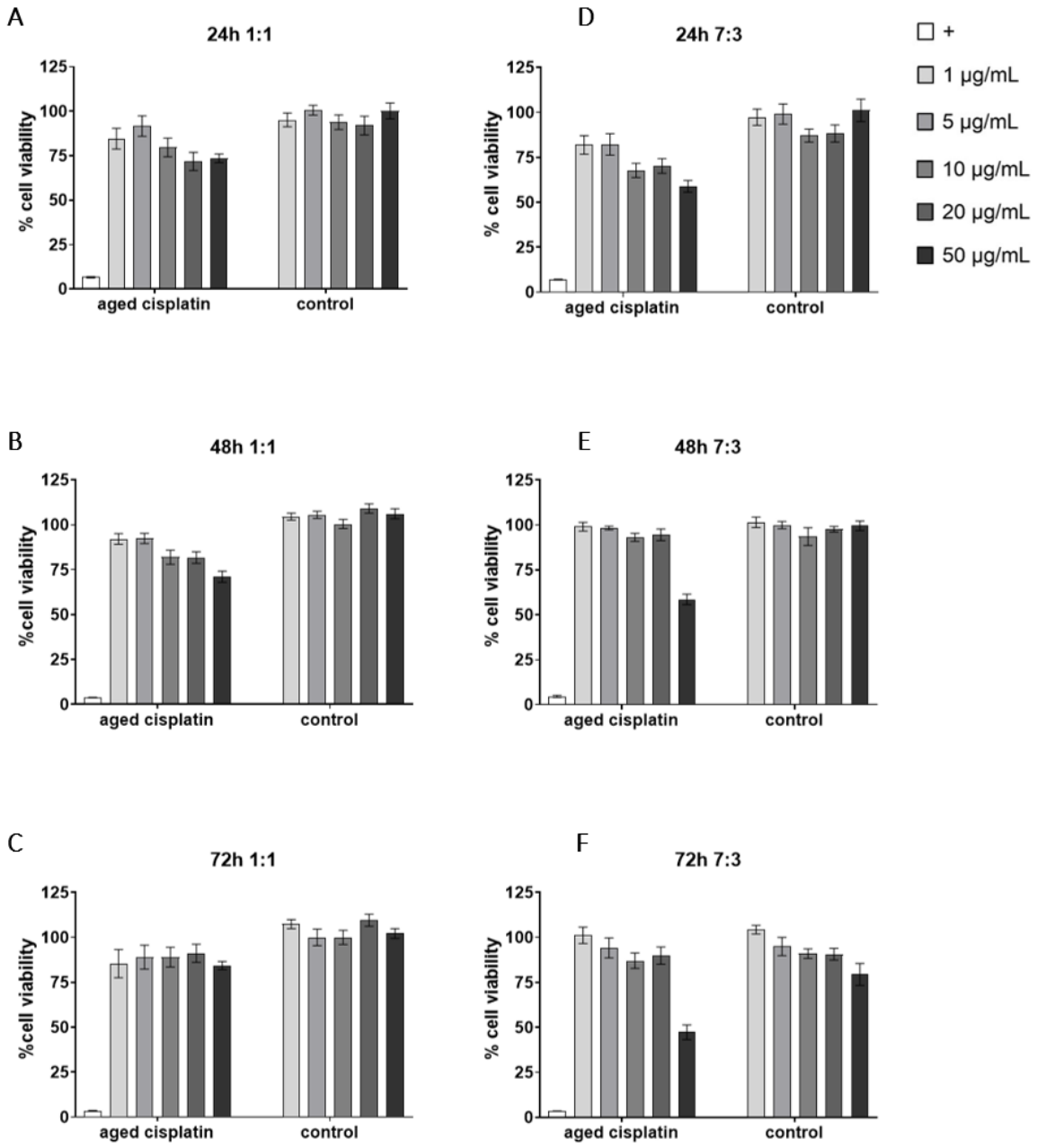

Fig. S2 – The effect of aged cisplatin samples compared to vehicle control. Cisplatin was dissolved in ratios of 1:1 and 7:3 of DMSO:H_2O solvent mixture and diluted to the indicated concentration range in culture medium. Samples were stored for one week in dark surroundings at 4°C. OSCC (n=3) were treated either with the aged dissolved cisplatin samples or the solvent vehicle (control). Cell viability was examined using the Alamar Blue assay following 24h, 48h, and 72h of exposure to dissolved cisplatin or vehicle in 1:1 **(A,B,C)** or 7:3 **(D,E,F)** ratios . Data were normalized to the untreated control and expressed as relative percentages. Data are represented as mean ± SEM. *OSCC, oral squamous cell carcinoma cell line (UM-SCC14c); DMSO, dimethylsulfoxide; +, positive control for cell death.*

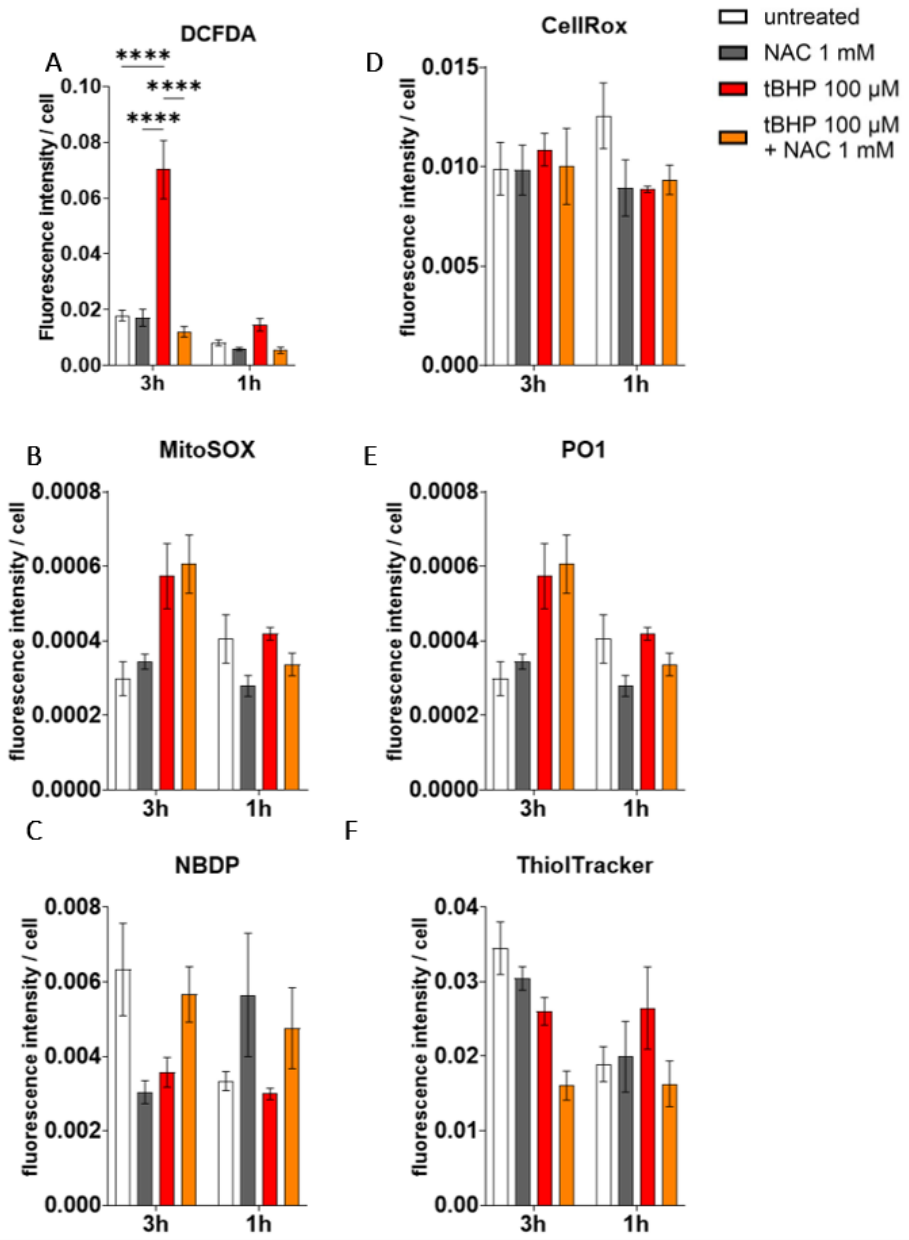

Fig. S3 – Detection of ROS or GSH through microplate assays. Microplate assays showing redox status evaluation in OSCC (n=3) treated with tBHP 100 µM by itself or in combination with the ROS inhibitor NAC 1 mM, or with NAC 1 mM by itself, both for 3h and 1h. General oxidative stress was visualized using DCFDA **(A)** and CellRox **(D)**, mitochondrial superoxide and hydrogen peroxide respectively using MitoSOX™ **(B)** and Peroxyorange1 **(E)**, and gluthathione and general thiol presence through NBD-P **(C)** and Thioltracker **(F)** respectively. Data are represented as mean ± SEM. Statistical analysis was performed using one-way ANOVA, followed by Tukey's multiple comparisons test. **p < 0,005, ***p < 0,001. *OSCC, oral squamous cell carcinoma cell line (UM-SCC14c); DCFDA, 2',7'-dichlorofluorescin diacetate; MitoSOX™,mitochondrial superoxide probe, NBD-P,GSH-specific on-off fluorescent probe; PO1, peroxyorange-1; tBHP, tert-butyl hydroperoxide; NAC, N-acetyl-L-cysteine.*